CLM-R263

CLM-R263

UKAEA

Report

A NEW HEAT TRANSFER MODEL FOR DENSITY STRATIFIED MOLTEN POOLS WITH INTERNAL HEAT SOURCES

THE TWOLAY CODE

J. Morgan

CULHAM LABORATORY
Abingdon, Oxfordshire
1986

C.18 Available from H.M.Stationery Officer Price £5.00

CLM-R263

A NEW HEAT TRANSFER MODEL FOR DENSITY STRATIFIED MOLTEN POOLS WITH INTERNAL HEAT SOURCES

THE TWOLAY CODE

J. Morgan
UKAEA, Culham Laboratory,
Abingdon, Oxon OX14 3DB

ABSTRACT

This paper presents a new model (coded in the TWOLAY computer program) of heat transfer from internally heated molten pools which are density stratified into two layers. TWOLAY results are presented which cover the most probable range of conditions appropriate to postulated severe accidents in a large modern PWR. These calculations are compared with those of a corresponding single-layer model. Relative to single-layer models, the two-layer model produces significantly enhanced lateral heat fluxes just below the upper surface of the pool. For this reason it is concluded that any predictive model of in-vessel thermal attack should provide for stratified pool heat transfer.

Although the model described here has been primarily developed for studies of in-vessel thermal attack it could, with suitable geometry modifications, be applied to other molten pool configurations. Although here applied to water reactor severe accident conditions, the model and code are also suitable for LMFBR applications.

October, 1985

ISBN 0853111 464

CONTENTS

1. INTRODUCTION

A conceivable consequence of a postulated severe accident in a nuclear reactor is the formation of a pool of molten debris. In general the formation of molten pools will lead to significant thermal loads on any contacting structure(s). In early studies of water reactor safety [1,2], in-vessel thermal attack was considered to be of significance only in as much as it affected the timing of ex-vessel events. Thus most thermal attack studies have concentrated on the ex-vessel phase of the accident i.e. core-concrete interactions. More recently, however, this emphasis has changed as a result of (1) the recognition of a dispersive mode of vessel failure [3,4] and (2) studies of debris conditions during the attack [5,6]. Thermal attack is now recognised as affecting (i) the mode of vessel failure, (ii) the quantity of debris released from the vessel and (iii) the debris temperature. The metallic debris fraction in (ii) is of special interest since it has significant effects on subsequent combustible gas production.

Models of in-vessel thermal attack have previously only considered heat transfer from a single homogeneous debris layer [5,7,8]. In reality, however, the molten debris is expected to be density stratified. (N.B. Models of the core-concrete interaction [e.g. 9,10] generally use multilayer heat transfer models and so historically the modelling of the in-vessel and ex-vessel accident phases has been inconsistent.) In-vessel single-layer models do, however, provide useful scoping calculations of thermal attack. This study shows that a density stratified two-layer model is necessary to provide the increased detail necessary for predictive calculations of the mode and timing of vessel failure.

In this paper details are given of a new model (coded in the TWOLAY computer program) for evaluating the heat transfer from in-vessel molten debris pools which are density stratified into two-layers. Calculations, performed with the model, are compared with the available experimental data. Results are also presented of a comparison study using

the TWOLAY code and the single-layer pool module of the MELTPV code [5]. The results of a preliminary version of this model, in simplified geometry, were presented in [6].

2. PHENOMENOLOGY AND MODEL FORMULATION

The formation and composition of molten debris pools is dependent on complex phenomena; discussions of the phenomenology of melt progression and hence melt pool formation are given in [11,6]. The pool composition is dependent on the details of the melt progression. In addition to fuel and its cladding (partly oxidised), quantities of steel and control rod material are also likely to be present.

The molten material is expected to be density stratified. This assertion is based on a number of experimental studies of the ternary U-Zr-O system [12,13,14]. These studies have indicated the likely formation of metallic and oxide like layers under the conditions conceivable in a severe accident. (As an example figure 1 shows the oxygen-stabilised zirconium and uranium dioxide phase diagram obtained by Politis [12].) In reality, the situation is likely to be more complex, with the addition of quantities of structural steel and control rod material. Based on the similar chemical properties, it is here assumed that this additional material segregates into the appropriate (metallic or oxidic) layer. (If required the model could be extended to model multi-layered configurations.)

A comprehensive review of heat transfer from internally heated fluid layers has been performed as part of the EEC study contract 'Compendium of Post Accident Heat Removal Models for Liquid Metal Cooled Fast Breeder Reactors' [15]. For a two-layer model the above review shows (1) only limited theoretical work has been reported [e.g. 16, 17] and (2) only a few density stratified, small scale simulant experiments (in rectangular geometry) have been performed [18,19]. The review in [15] reports that data for steady state heat transfer from a single internally heated layer, of infinite extent, with an adiabatic lower boundary, may be correlated by,

$$Nu = C(Ra_q)^{\gamma} \qquad (1)$$

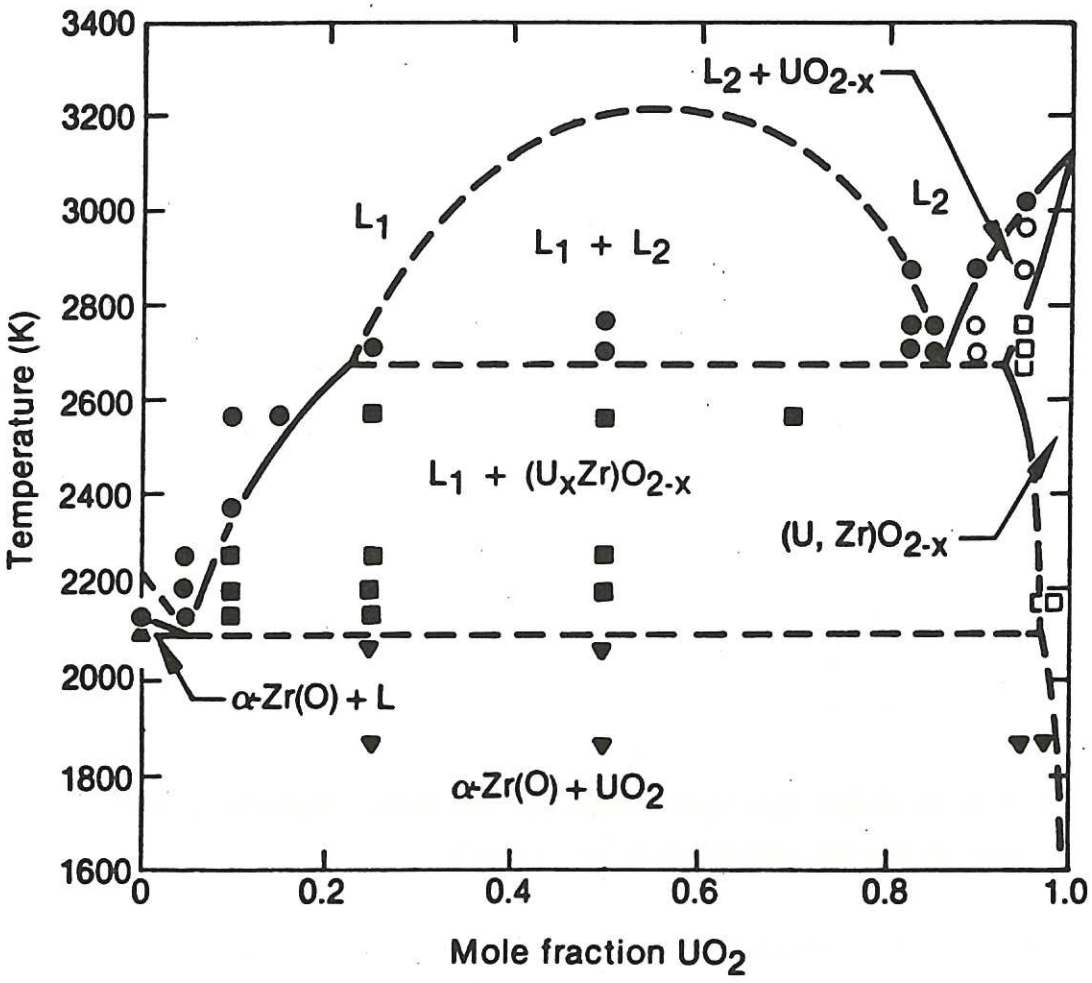

Figure 1 Oxygen Stabilised, Alpha Phase Zirconium–Uranium Dioxide Quasi–Binary Phase Diagram, According to Poltis.

where,

$Nu \equiv$ Nusselt Number $\left(= \frac{\phi L}{k\Delta T}\right)$

$Ra_q \equiv$ Modified Rayleigh Number $\left(= \frac{\beta g q L^5}{\alpha \nu k}\right)$

$\phi \equiv$ Heat flux across a surface (geometry not yet specified)

$L \equiv$ Layer thickness

$k \equiv$ Thermal conductivity

$\Delta T \equiv$ Temperature difference between bulk and surface

$\beta \equiv$ Coefficient of thermal expansion

$g \equiv$ Acceleration due to gravity

$q \equiv$ Volumetric heating rate

$\nu \equiv$ Kinematic viscosity

$\alpha \equiv$ Thermal diffusivity $\left(= \frac{k}{\rho c}\right)$

$c \equiv$ Specific heat capacity

$\rho \equiv$ Density

$C, \gamma \equiv$ Constants

(N.B. The modified Rayleigh number is the usual Rayleigh number rewritten in terms of the volumetric heating rate.)

The above Nusselt-Rayleigh number relation is just one of a number of dimensionless groupings which have been used to correlate natural convection heat transfer data. Although this grouping is probably the most popular for natural convection studies, other dimensionless groups can be used. As an example, liquid metal heat transfer correlations have been produced which are based on the Boussinesq number (Bo). These correlations have the same form as equation (1) i.e.

$$Nu = A\,(Bo)^m$$

where

$$Bo = Gr\ Pr^2$$

$Gr \equiv$ Grashof number $\left(= \frac{g\beta\Delta T L^3}{\nu^2}\right)$

$Pr \equiv$ Prandtl number $\left(= \frac{\rho \nu c}{k}\right)$

A,m = constants

Notice that viscosity does not appear in the Boussinesq number. Correlations using this number were developed on the basis that liquid metals have a low Prandtl number and therefore the viscosity, in large volumes of liquid, should not be important. A Boussinesq number correlation has not, however, been adopted in this study for the metallic layer model. This decision was based on the following considerations

(1) Typical Prandtl numbers for molten metallic debris are about 0.05 to 0.10. When used in the correlations based on the Boussinesq number, the resulting Nusselt numbers are similar to those produced by correlations based on the Rayleigh number. Usually the difference between these correlations is approximately the same as the uncertainty in the experimental data.

(2) Most experimental studies of liquid metals have been performed with Boussinesq numbers in the range 10^3 to 10^6. Typical postulated severe accident conditions are, however, likely to result in Boussinesq numbers of about 10^{13}. The extrapolation of such correlations by so many orders of magnitude is obviously unreliable. However the experimental basis of the Nusselt-Rayleigh correlations extends to Rayleigh numbers within about two orders of magnitude of the typical value for severe accident conditions ($\sim 10^{14}$).

If the heat transfer from a layer can be correlated by an expression of the form of equation (1), then [5],

$$\frac{\phi L}{k\Delta T} = C\left(\frac{\beta g q L^5}{\alpha \nu k}\right)^{\gamma}$$

substitution of $\phi = qL$ gives,

$$\frac{\phi L}{k\Delta T} = C\left(\frac{\beta g \Delta T L^3}{\alpha \nu}\right)^{\gamma} \cdot \left(\frac{\phi L}{k\Delta T}\right)^{\gamma} \quad , \quad \text{or}$$

$$\phi = \frac{k}{L}\left[C\left(\frac{\beta g \Delta T L^3}{\alpha \nu}\right)^{\gamma}\right]^{\left(\frac{1}{1-\gamma}\right)} \Delta T \qquad (2)$$

Equation (2) represents the heat flux obtained from the steady state correlation but rewritten in terms of the temperature difference across the thermal boundary layer. It has been suggested that such a correlation also gives the transient heat flux before steady state is reached [5]. Heat flux calculations, using equation (2), have been compared in [15] with the transient measurements reported by Kulacki et al. [20]. The agreement is at least as good as that between other correlations and the steady-state data.

The heat flux given by equation (2) represents the upwards transfer of heat from an infinite horizontal fluid layer on an adiabatic surface. In most relevant applications all the pool boundaries are isothermal. Both Peckover [21] and Baker et al. [22] have suggested that the fluid layer may be considered as consisting of upper convecting and lower conducting sub-layers separated by the (mathematical) surface on which the temperature is a maximum, which plays the role of an adiabatic boundary. The convective motion in the upper sub-layer is assumed to have little effect on the heat conduction across the stable lower sub- layer. The present model is based on this assumption and the heat flux from the convection sub-layer is correlated using the 'adiabatic' equation (2).

Figure 2 shows a schematic representation of the TWOLAY model. The pool is modelled in hemispherical geometry with molten metal overlying the oxide. The user specifies debris quantities and thermophysical properties, together with a choice of upper surface boundary condition. (Although not currently implemented in TWOLAY, the MATPRO [23] subroutine library could be used to provide properties of the 'U-Zr-O' system.) Heat may be lost from the upper surface either by radiation or by boiling of an overlying coolant. Figure 2 shows solid debris crusts at both the metal upper surface and at the internal interface; these crusts are shown simply to illustrate that TWOLAY is capable of considering their formation and effect: they are <u>not</u> necessarily assumed to form.

Debris which is released from the core will, in general, contain all but the most volatile fission products (volatiles typically account for about 20% of the total fission product heating). Details of the quantitative segregation of the fission products with individual debris constituents are uncertain. To allow for this uncertainty TWOLAY requires the user to specify the respective fractions of the total 'whole core' fission product heating in each layer. The total debris decay heat may be calculated using the ANS standard [24]. N.B. This is not the latest decay heat standard, but the use of the current ANS formulation is not expected to produce significant differences in TWOLAY results.

3. DETAILED MODEL DESCRIPTION

This section contains a detailed description of the equations solved in the TWOLAY code.

3.1 Oxide Layer Equations

Heat transfer in the oxide (lower) layer is modelled using the previously reported single layer model [5]. The model assumes the existence of conduction and convection sub-layers. Heat is transferred upwards and sidewards from the convection sub-layer and downwards from the conduction sub-layer. In the hemispherical geometry used here, the terms 'sidewards' and 'downwards' are somewhat subjective. A 'downwards' heat flux refers to the transfer of heat from the conduction sub-layer to the adjacent pool boundary (see figure 2). Similarly the 'sidewards' heat flux is the transfer of heat from the convection sub-layer in a lateral direction.

Equation (2) applied to the oxide upwards heat flux gives,

$$\phi^{u}_{ox} = \frac{k_{ox}}{L_{ox}}\left[C^{u}_{ox}\left(\frac{\beta_{ox} g (T^{Bulk}_{ox} - T^{I}_{ox}) L^{3}_{ox}}{\alpha_{ox}\nu_{ox}}\right)^{\gamma^{u}_{ox}}\right]^{\frac{1}{(1-\gamma^{u}_{ox})}} (T^{Bulk}_{ox} - T^{I}_{ox})\, x^{\delta} \qquad (3)$$

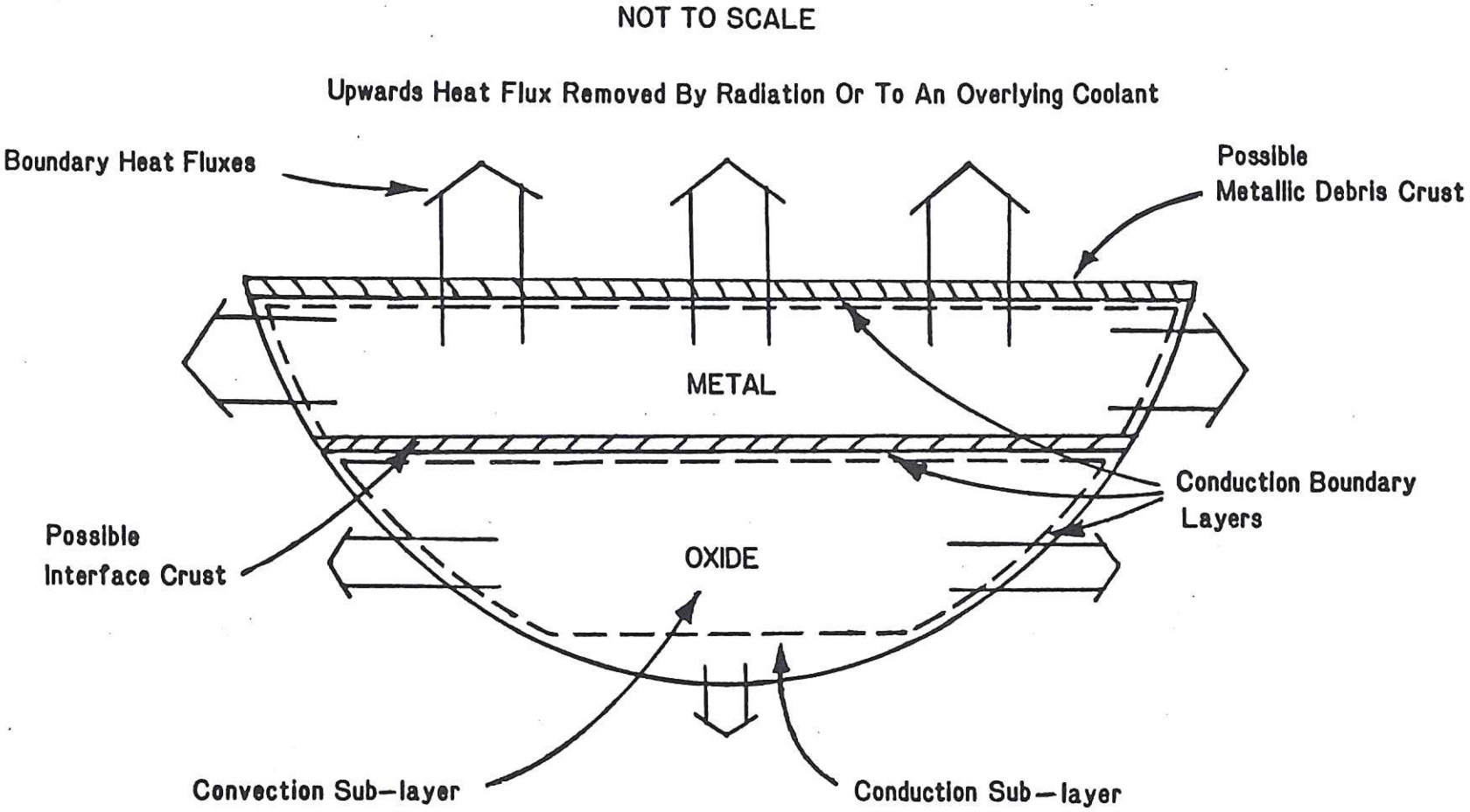

Figure 2 Schematic Representation of the TWOLAY Model

where

T_{ox}^{I} ≡ Oxide interface temperature

$$\delta = \frac{(4\gamma_{ox}^{u} - 1)}{(1 - \gamma_{ox}^{u})}$$

x ≡ Fraction of the oxide layer depth which is convecting

Similarly an expression of this form may be obtained for the sidewards oxide heat flux, using an appropriate heat transfer correlation and a driving temperature difference of the 'bulk' temperature minus that at the side ($T_{ox}^{Bulk} - T_{ox}^{s}$). (In this study, the calculations use the same sidewards as upwards heat transfer correlation. This approximation is based on the review in [15] which noted the similarity in the measured upwards and sidewards heat transfer data.) The downwards heat flux from the oxide is simply,

$$\phi_{ox}^{d} = \frac{2k_{ox}(T_{ox}^{Bulk} - T_{ox}^{d})}{(1 - x)\, L_{ox}} \qquad (4)$$

where

T_{ox}^{d} ≡ Oxide temperature at the bottom.

The fraction of the oxide layer depth which is convecting (x), may be calculated by the same method used in the single-layer model [5].

The above heat flux expressions may then be used in the enthalpy balance (equation 5) to give the oxide bulk temperature.

$$M_{ox} c_{p}^{ox} \frac{dT_{ox}^{Bulk}}{dt} = QDK_{ox} - \phi_{ox}^{u} A_{I} - \phi_{ox}^{s} A_{ox}^{s} - \phi_{ox}^{d} A_{ox}^{d} \qquad (5)$$

where

M_{ox} ≡ Oxide mass

c_p^{ox} ≡ Oxide specific heat capacity

T_{ox}^{Bulk} ≡ Oxide bulk temperature

QDK_{ox} ≡ Decay heat of the oxide

ϕ_{ox}^{u}, ϕ_{ox}^{s}, ϕ_{ox}^{d} ≡ Upwards, sidewards and downwards, heat fluxes from the oxide

A_{ox}^{s}, A_{ox}^{d} ≡ Sidewards and downwards heat transfer areas

A_I ≡ Metal/Oxide interface area

3.2 Metal Layer Equations

The upwards and sidewards heat fluxes from the metal may similarly be represented by analogous expressions of the form (3). (For these expressions x=1 since all the layer is assumed to be convecting.)

For the metallic layer the enthalpy balance is as follows,

$$M_{met} c_p^{met} \frac{dT_{met}^{I}}{dt} = QDK_{met} - \phi_{met}^{u} A_{met}^{u} - \phi_{met}^{s} A_{met}^{s} + \phi_{ox}^{u} A_I \qquad (6)$$

where

M_{met} ≡ Mass of metal

c_p^{met} ≡ Metal specific heat capacity

T_{met}^{I} ≡ Metal interface temperature
= Metal bulk temperature

QDK_{met} ≡ Metal decay heat

ϕ_{met}^{u}, ϕ_{met}^{s} ≡ Upwards and sidewards heat fluxes from the metal

A^{u}_{met}, A^{s}_{met} ≡ Upwards and sidewards heat transfer areas

3.3 Metallic Upper Surface Boundary Condition

At the upper surface of the metal (be it solid or molten at temperature T^{T}, two boundary conditions are possible. These are (i) heat transfer to overlying water and (ii) radiation to structures above the debris.

For the first of these, heat is removed by a combination of film boiling and radiation (to the water saturation temperature, T^{sat}). The overall heat-transfer coefficient (h) in this situation has been reported [25] as,

$$h = h_{FB}\left[\frac{h_{FB}}{h}\right]^{1/3} + h_{R} \qquad (7)$$

where

h_{R} ≡ Radiation heat transfer coefficient (treating the water as a black body absorber)

$$= \frac{\sigma_{SB}\varepsilon\left[(T^{T})^{4} - (T^{sat})^{4}\right]}{T^{T} - T^{sat}}$$

σ_{SB} ≡ Stefan-Boltzman constant

ε ≡ Emissivity of the radiating surface

and

$$h_{FB} = 0.42\left[\frac{k_{v}^{3}\rho_{v}(\rho_{\ell} - \rho_{v})\lambda g}{\mu_{v}(T^{T} - T^{sat})\left\{\frac{\sigma}{g(\rho_{\ell} - \rho_{v})}\right\}^{1/2}}\right]^{1/4}$$

k_{v} ≡ Vapour thermal conductivity

ρ_{v} ≡ Vapour density

ρ_{ℓ} ≡ Liquid density

λ ≡ Latent heat of vaporisation

μ_{v} ≡ Vapour viscosity

σ ≡ Surface tension

N.B. All vapour thermal properties for the film boiling heat transfer coefficient should be evaluated at the film temperature

$$T_F = 0.5(T^T + T^{sat}).$$

In the absence of overlying coolant heat is transferred upwards by radiation. For this calculation a heat transfer coefficient similar to h_R (in equation (7)) is used, but with a user supplied sink temperature in place of T^{sat}.

3.4 Interfacial and Upper Crust Calculation

In the TWOLAY code a crust of solid (oxide) lower layer material can form at the interface between the two layers. Interface crusts can only form if the upper layer has a bulk temperature below the lower layer's melting point. For typical severe accident conditions, with metallic over oxide debris, interface crust formation is expected. (The long term dynamic stability of such crusts is, however, uncertain - TWOLAY assumes stable crust formation). Crust formation at the layer interface affects the upwards heat transfer. In the presence of a crust the upper boundary of the molten lower layer is at its melting point. Without a crust the upper surface temperature is only constrained by the upper layer enthalpy balance.

Crust formation is also possible at the top of the upper (metallic) layer. Upper layer material may freeze at this boundary if upwards heat transfer is sufficiently good that the top surface temperature drops below the metallic layer melting point. Upper crust formation similarly affects the heat transfer from the upper layer. In equilibrium, without crust formation, the higher upper boundary temperature results in reduced upwards heat transfer from the layer (relative to the equivalent case with an upper crust). The reduced upwards heat transfer leads to a higher bulk layer temperature and therefore increased sidewards heat transfer.

To calculate the interfacial and upper crust thicknesses the steady-state approximation is used.

$$s = \frac{k\Delta T}{\phi} \qquad (8)$$

where

s = Crust thickness

k = Thermal conductivity of the crust

ϕ = Heat flux across the crust

ΔT = Temperature difference across the crust.

For transient calculations, this is usually a good approximation since the timescales of interest are much larger than the thermal timescale for a crust to develop. If required it would, however, be possible to replace this approximation with a transient calculation such as that described in [5].

4. NUMERICAL SOLUTION SCHEME

The equations given for this model include transient terms. (This scheme was primarily chosen so that the model can eventually be incorporated into an improved version of the MELTPV code [5].) In this paper, only steady state calculations are presented with 'time' advanced until the layers reach a configuration of constant heat transfer to their respective boundaries. The decay heat is held constant throughout the calculation, being evaluated at a user specified time. Brief details of the calculational route used, in TWOLAY, are given below:-

a) Evaluate the volume of metallic and oxidic debris. Also calculate the layer depths and surface areas.

b) Use the ANS decay heat formulation to evaluate the total 'core' decay heat at the user specified accident time. Then work out the fission product heating in each layer.

c) Calculate the fraction of the oxide layer depth (x) which is convecting.

d) Use x to calculate the oxide boundary heat fluxes. (Note the respective 'sidewards' and 'downwards' heat transfer areas are dependent on x.)

e) Perform an oxide layer enthalpy balance to produce the bulk layer temperature.

f) Calculate the thickness of the debris interface crust (if it exists). Similarly if an upper surface crust exists calculate its thickness. For both crusts work out the temperature difference across them.

g) Evaluate the molten metal upper surface temperature using the appropriate upper surface heat transfer model.

h) Determine the upwards and sidewards heat fluxes from the metallic debris layer.

i) Perform an enthalpy balance for the metallic bulk layer temperature.

j) Calculate the top surface temperature of the metal if a crust has formed.

k) Output current 'timestep' values, advance 'time' and repeat above sequence from (c). Continue calculation until all temperatures have reached equilibrium (i.e. until constant to within the user required relative error).

The algorithm described above is not optimised in TWOLAY. (This is a consequence of the somewhat arbitrary method used to increase the timestep as the calculation progresses.) Nevertheless the program is very quick and cheap to run. Typically, the calculations presented in sections 6 and 7 of this paper each used less than 10 CPU seconds on the Culham PRIME 9950 computer. (For these calculations a relative error of 10^{-4} was used to define both convergence and accuracy.)

5. MODEL VALIDATION

In this section calculations using the model described in this report are compared with experimental data.

The heat transfer review in [15] revealed only two relevant experimental studies, i.e. [18,19]. Both studies used simulant materials in small scale rectangular geometry. The investigations further differ from the more general situation, described here, by having adiabatic lower and side

boundaries, and heat generation in only the lower layer. The results of these studies were correlated using an expression of the form of equation (1) but with an effective upwards Nusselt number (Nu*) together with the modified Rayleigh number for the lower layer (Ra_{qB}). The effective Nusselt number is based on the effective thermal conductivity k_e of the combined layer i.e.

$$Nu^* = \frac{h\,(L_T + L_B)}{k_e}$$

with

$$k_e = \frac{(L_T + L_B)}{\frac{L_T}{k_T} + \frac{L_B}{k_B}}$$

and

$$h = \frac{\phi}{(T_B - T_T)}$$

where

$L_T \equiv$ Upper layer thickness
$L_B \equiv$ Lower layer thickness
$k_T \equiv$ Upper layer thermal conductivity
$k_B \equiv$ Lower layer thermal conductivity
$T_T \equiv$ Upper surface temperature
$T_B \equiv$ Lower surface temperature

Considering the lower layer separately, Ra_{qB} is the modified Rayleigh number as defined for equation (1) i.e. it uses only the lower layer depth and thermophysical properties.

Table 1, reproduced from [15], summarises the correlations given in [18,19].

The model described in this paper has been compared against the detailed experimental measurements given in [19]. In this study two convection

chambers were used, with base dimensions of 25.4 x 25.4 cm and 50.8 x 50.8 cm respectively. Twenty cases were chosen, the first twelve of which correspond to the minimum and maximum Rayleigh number for each of the six correlations from [19]. The remaining cases were chosen at random. (Only three of these experiments used the small test cell i.e. numbers 807, 601 and 401B.) These experiments were all performed with an isothermal upper boundary (i.e. using a cooled plate). For each calculation the top surface temperature was therefore fixed to that measured in the appropriate experiment. Similarly each calculation has the same heat generation rate as the corresponding experiment. Table 2 summarises the measured and calculated interface and bottom surface temperatures. Details of the experimental measurements are given in Appendix B of [19]. Some inconsistency is, however, noted between the power input and volumetric heating rate for experiments 710, 504 and 305 given in [19]. It is not possible to determine from the data given in Appendix B which of these is correct. For the purpose of this study the comparison calculations are based on the stated power input.

The calculated temperatures show relatively good agreement with the experimental measurements. It is, however, the temperature differences across each layer that control heat transfer; in most cases the agreement here is only reasonable. Table 2 also shows a comparison of the experimental and theoretical values for the effective Nusselt number (Nu*); the relatively good agreement is highlighted by the comparison of Figure 3.

Although the results of the above comparison are encouraging there is still a need for further experimental data to validate the model. This is particularly necessary for the more general situation of internal heating in both sub-layers and with heat transfer to all the pool boundaries.

6. PARAMETER AND COMPARISON STUDY

The two-layer model described above has been used for a parameter study. For each parameter variation a comparison calculation has also been performed using the equivalent single-layer module of the MELTPV code

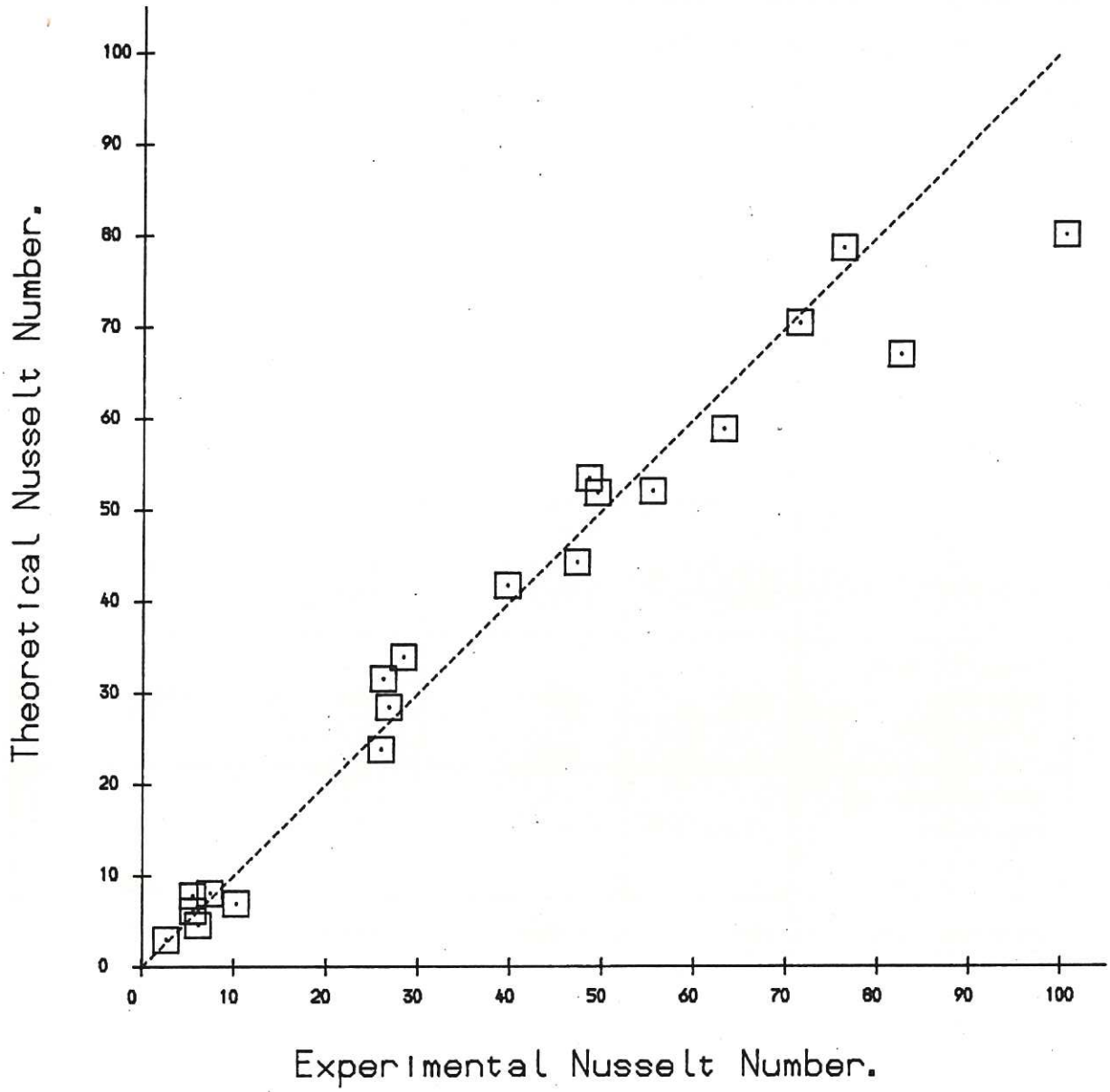

Figure 3 Comparison of Theoretical and Experimental Nusselt Numbers for the Density Stratified Study of Kulacki and Nguyen.

[5]. The data used for these calculations are based on a large modern PWR design. Specifically the calculations assume a whole core containing 101 tonnes of uranium dioxide, 21 tonnes of zirconium and 5 tonnes of miscellaneous core metal (treated as steel). The total decay heating is set to 28.2 MW. (This figure was obtained using subroutine ANSQ of the MARCH code [7] and applies to the whole core two hours after the start of the accident.)

Thermophysical properties for the metallic and oxide layers are calculated by means of mass or volume averages using the following data.

	Metallic Debris		Oxide Debris	
	Stainless Steel	Zirconium	Zirconium Dioxide	Uranium Dioxide
Specific Heat Capacity ($J\ kg^{-1}K^{-1}$)	600	367	815	503
Coefficient of Expansion (per K)	17.6×10^{-5}	*	*	7.4×10^{-5}
Density ($kg\ m^{-3}$)	6917.	6180.	5990.	9850.
Thermal Conductivity ($W\ m^{-1}K^{-1}$)	22.3	36.	1.4	3.5
Viscosity ($kg\ m^{-1}s^{-1}$)	1.6×10^{-3}	*	*	4×10^{-3}

Note: For the omissions marked with an asterisk, no information was available and therefore the corresponding steel or uranium dioxide data was used for the respective 'metallic' or 'oxide' layer.

The parameters varied in the study are as follows:

(1) The fraction of the total core used. As a base case half the core molten is considered, but calculations are presented with up to the whole core molten.

(2) Partition of decay heating between the two layers. In general the majority of the fission product heating is expected to be in the oxide layer. Here, the base case for the ratio of metal to oxide heating is taken as 1:2. Further calculations are also included which vary from all the heating in the oxide layer to equal heating in both layers.

(3) Fractional oxidation of the zirconium debris. In this study it is generally assumed that 30% of the core zirconium has been oxidised before it reaches the lower head. Two additional calculations using 60% and 100% oxidised are also presented.

(4) Upper surface heat transfer. Calculations are shown with upwards heat transfer either to an overlying coolant or by radiation to above pool structures.

(5) Additional steel mass added to the debris. This corresponds to the mass of ablated structures added to the debris. In these calculations this is varied between 0 and 10 tonnes.

The correlation used for the upwards and sidewards heat transfer is due to Kulacki and Emara [26]. This correlation is recommended in [15] for this application, largely on the basis of its validity at higher modified Rayleigh numbers (i.e. up to about 10^{12}).

The parameter study matrix is shown in Table 3 and the detailed TWOLAY NAMELIST input is described in Appendix A.

7. DISCUSSION OF THE STUDY RESULTS

Table 4 shows TWOLAY results together with those of the single-layer model. In this section corresponding results obtained with the single-and two-layer models are discussed. This is followed by a discussion of the TWOLAY parameter study.

In most cases the results obtained from the two-layer model show an enhanced heat flux from the metallic layer over that from the oxide layer For some cases the respective 'oxide' and 'metallic' heat fluxes differ by over an order of magnitude. Heat fluxes calculated by the single-layer model only marginally exceed (by up to a factor of about two) the corresponding 'oxide' layer heat flux, obtained with the two-layer model. This similarity extends to the downwards heat flux calculated by both models. (Results from both models show the downward heat flux to be typically an order of magnitude lower than other boundary heat fluxes.) The results presented (in Table 4) for the upwards heat flux, calculated by the two models, show a larger upwards heat transfer from the single-layer model. Results for the single layer model show the same upward and sideward heat fluxes as a consequence of the formation of an upper surface crust. (N.B. The existence of an upper crust leads to the same upwards and sidewards temperature difference, within the pool, and hence the same heat flux when using the same heat transfer correlations.) In all the two-layer calculations a solid oxide crust forms at the layer interface. (Crust formation at the metallic surface is discussed in (iv) below.)

For the single-layer model the bulk pool temperature varies from about 150 to 350°C above its (input) melting point. In each case the single-layer has a calculated bulk temperature similar to that of the corresponding TWOLAY result for the oxide layer. A slightly wider variation is evident in the TWOLAY calculations for the metallic layer bulk temperature i.e. the temperatures vary from about 50 to 350°C above the (input) metallic debris melting point.

In the remainder of this section results of the parameter study are discussed. The following five points correspond to those in section 6 above.

(i) Increasing the volume of pool material leads to higher convective heat fluxes. This is a consequence of the increased volume to surface area ratio of the larger pool.

(ii) The apportioning of the fission product heating between the oxide and metallic layers has a significant effect on the boundary heat fluxes (total decay heating constant). As expected the heat fluxes from each layer increase with the fission product heat input. For all the cases considered, the sidewards heat fluxes from the metallic layer are considerably larger than those from the oxide. The increase in heat flux with heat generation is reflected in the calculated bulk temperatures. The relatively large variations in heat fluxes are produced by small changes in the bulk temperature. (This is because the 'driving' quantity, in the heat transfer mechanism, is the temperature difference between the bulk and boundary.)

(iii) In the calculations reported here, the fraction of zirconium (cladding) oxidised has a large impact on the pool heat transfer. As the fraction oxidised rises, the metallic boundary heat fluxes increase sharply. This is mainly due to the constant, metallic layer, fission product heating assumed. As a result of this, at the same fission product heating rate, a decrease in the metallic volume implies an increase in volumetric heat source. This in turn explains the large increase in the boundary heat fluxes. The fraction of oxidised clad has a minimal effect on the calculated oxide bulk temperature. For the metallic layer, the bulk temperature increases sharply with the fraction oxidised. The data set with all the clad oxidised produced the highest sidewards heat flux from the metallic layer obtained in this study.

(iv) The effect of the upper surface boundary condition is now discussed. All the calculations so far described have used the radiation heat transfer model at the pool upper surface. To remove the upwards heat fluxes calculated, temperatures in excess of the metallic debris melting point are necessary i.e. no upper crust forms. This is in contrast to the majority of the calculations

performed with overlying water. In these calculations the water is able to remove (by film-boiling) a greater heat flux from the debris. As a consequence the upper surface temperature drops below the metallic debris melting point and an upper crust froms. The enhanced heat removal capability of overlying water has a significant effect on the sidewards heat transfer from the metal. Inspection of Table 4 shows the respective sidewards heat fluxes to be the lowest obtained in the study. In the last calculation performed, with water overlying debris from the whole core, the upwards heat flux is sufficiently great as to prevent crust formation. The sidewards heat flux from the metal is, however, considerably reduced compared to all the calculations with radiative heat transfer.

(v) The addition of steel to the metallic debris has the effect of reducing the heat fluxes from the upper layer. (As expected the calculations show no effect on the oxide layer.) The reduction in the upwards and sidewards heat fluxes is reflected in the metallic bulk temperature. Increasing the steel content of the metallic debris has the effect of reducing the volumetric heat input to the layer. (In these calculations the ratio of fission product heating between the two layers is constant.)

8. CONCLUSIONS

Recent severe accident studies have highlighted the need for predictive models of in-vessel thermal attack from molten debris.

Previous models of in-vessel thermal attack from molten debris have assumed the molten pool to be a homogenous mixture. In this report a new heat transfer model, with density stratification of the pool, is presented. (The model described here, and implemented in TWOLAY, has only one 'metallic' layer and one 'oxide' layer. It could, however, be extended into a multi-stratified configuration.)

Calculations are presented which demonstrate, good agreement with available experimental measurements. Although this agreement is encouraging there is a need for further, larger scale, confirmatory experiments with more appropriate materials and heat transfer conditions. Calculations are also described which show that segregation of the debris, into two layers, significantly affects the quantitative predictions of the boundary heat fluxes. Comparisons are made with results obtained using an equivalent single- layer model. Relative to the homogenous single-layer model, the two-layer model produces enhanced lateral heat fluxes just below the upper surface of the pool. In the majority of cases considered, the respective heat fluxes differ by over an order of magnitude.

The TWOLAY code has also been used to study the effects of fission product segregation, different heat removal mechanisms at the upper boundary and debris quantity/composition. All these factors play a large part in determining the boundary heat fluxes. Probably of most interest is the observation that lateral heat fluxes from the 'metallic' layer are reduced (to comparable single-layer values) for situations with an overlying coolant. This is a consequence of the formation of an upper surface debris crust resulting from the increased upwards heat transfer.

The large discrepancies between the single- and two-layer model predictions show the importance of density stratification on the overall heat transfer from the debris. Therefore, it is recommended that all predictive models of in-vessel thermal attack should include density stratified layers. In-line with this recommendation the relevant parts of TWOLAY will be incorporated into the MELTPV code [5,11].

9. ACKNOWLEDGEMENT

The author would like to thank Dr. B. Turland and Dr. F. Briscoe for helpful discussions during the preparation of this paper.

Table 1. Effective Nusselt Number Correlations for the Two Layer Experiments of Kulacki et al. [18,19].

C	M	Range of Rayleigh number, Ra_{qB}	Range of Prandtl numbers, Pr_T, Pr_B	Layer Geometry: Aspect Ratio $(\frac{L}{D})$ Layer Depths Ratio $(\frac{L_T}{L_B})$	Fluid Used	Authors
0.254	0.228	$3.4 \times 10^4 - 9.5 \times 10^{10}$	$\frac{Pr_T}{Pr_B} \simeq 12$	$\frac{L_T}{L_B} = 0.433$	Silicon Oil upper layer with a copper sulphate solution lower layer	Kulacki and Nguyen
0.286	0.196	$3.8 \times 10^6 - 3.0 \times 10^{11}$	$Pr_B \simeq 7$	$\frac{L_T}{L_B} = 0.110$		
0.244	0.194	$9.3 \times 10^7 - 4.2 \times 10^{11}$		$\frac{L_T}{L_B} = 0.035$		
0.269	0.233	$8.7 \times 10^5 - 4.1 \times 10^{10}$	$\frac{Pr_T}{Pr_B} = 1$	$\frac{L_T}{L_B} = 0.433$	Heptane upper layer with a copper sulphate solution lower layer	
0.171	0.227	$1.6 \times 10^7 - 1.6 \times 10^{11}$	$Pr_B = 6.5$	$\frac{L_T}{L_B} = 0.110$		
0.129	0.230	$1.1 \times 10^7 - 2.1 \times 10^{11}$		$\frac{L_T}{L_B} = 0.035$		
0.264	0.225	$3.4 \times 10^4 - 9.5 \times 10^{10}$	$\frac{Pr_T}{Pr_B} = 11.8$	$\frac{L_T}{L_B} = 0.433$	Silicon Oil upper layer with a copper sulphate solution lower layer	Kulacki, Min, Nguyen and Keyhani
0.262	0.199	$3.8 \times 10^6 - 3.1 \times 10^{11}$	$Pr_B = 6.3$	$\frac{L_T}{L_B} = 0.110$		
0.250	0.192	$9.3 \times 10^7 - 4.5 \times 10^{11}$		$\frac{L_T}{L_B} = 0.035$		

Various aspect ratios $0.05 \leq \frac{L}{D} \leq 0.50$; D = 50.8cm; Thickness = 50.8cm

Various aspect ratios $0.20 \leq \frac{L}{D} \leq 0.50$; Small cell: D=25.4cm Thickness = 25.4cm; Large cell: D=50.8cm Thickness = 50.8cm

Various aspect ratios; D=50.8cm Thickness = 50.8cm

Table 2: Comparison calculations, obtained with the new heat transfer model, for the experimental data of Kulacki and Nguyen [19]

Test Number in [19]	Measured Top Surface Temperature (°C)	Interface Temperature (°C)		Bottom Temperature (°C)		Nusselt Number	
		Expt.	Calc.	Expt.	Calc.	Expt.	Calc.
55A	23.86	24.19	24.15	24.29	24.24	2.64	2.98
94B	31.47	41.54	43.44	47.31	46.81	76.02	78.58
77B	24.38	24.48	24.53	24.54	24.59	6.12	4.59
86B	28.19	40.44	41.24	46.09	45.26	49.34	51.86
84	39.12	39.55	39.88	39.83	40.16	10.25	6.93
107A	35.04	44.48	46.01	49.06	49.74	47.12	44.25
807	22.91	23.22	23.19	23.50	23.33	5.52	7.82
710	29.22	35.01	35.09	36.12	37.88	100.41	79.96
601	23.08	23.58	24.10	24.82	24.68	7.41	8.08
504	27.69	33.10	34.19	37.28	37.68	63.06	58.80
401B	23.11	23.33	23.69	24.14	24.05	5.56	6.16
305	24.80	30.57	31.34	34.75	35.28	55.32	52.04
97	25.30	27.09	27.34	28.13	27.99	39.60	41.70
93	27.22	27.38	28.27	28.54	28.65	25.91	23.81
109	29.11	31.91	31.84	33.14	32.90	26.74	28.46
703	24.34	26.47	25.82	26.74	26.52	48.39	53.45
501B	23.96	25.17	24.85	25.65	25.36	26.12	31.56
303B	21.37	23.42	22.98	24.48	23.98	28.28	33.92
709	26.41	29.83	29.70	30.39	31.30	82.27	66.95
98	30.52	38.56	40.57	43.20	43.35	71.27	70.41

Table 3 Details of the TWOLAY Parameter Study.

Parameter Study No.	PARAMETER VARIATIONS				
	Fraction of Core	Fraction Zr Oxidised	Ratio of Decay Heating in Metal to that in Oxide	Overlying Coolant	Additional Steel (Tonnes)
1	0.50	0.3	All in Oxide	No	None
2	0.50	0.3	1:1	No	None
3	0.50	0.3	1:2	No	None
4	0.50	0.3	1:10	No	None
5	0.75	0.3	1:2	No	None
6	1.00	0.3	1:2	No	None
7	0.50	0.6	1:2	No	None
8	0.50	1.0	1:2	No	None
9	0.50	0.3	1:2	No	5
10	0.50	0.3	1:2	No	10
11	1.00	0.3	1:2	No	10
12	0.50	0.3	All in Oxide	Yes	None
13	0.50	0.3	1:2	Yes	None
14	1.00	0.3	1:2	Yes	None

Table 4. Results Obtained with the TWOLAY Code.

Parameter Study No.	TWO LAYER MODEL						SINGLE LAYER MODEL			
	Oxide Sidewards Heat Flux ($MW\ m^{-2}$)	Metal Sidewards Heat Flux ($MW\ m^{-2}$)	Upwards Heat Flux ($MW\ m^{-2}$)	Downwards Heat Flux ($MW\ m^{-2}$)	Oxide 'Bulk' Temp. (°C)	Metal 'Bulk' Temp. (°C)	Sidewards Heat Flux ($MW\ m^{-2}$)	Upwards Heat Flux ($MW\ m^{-2}$)	Downwards Heat Flux $MW\ m^{-2}$)	Bulk Temp. (°C)
1	0.59	2.29	0.16	0.03	2805	1592	0.80	0.80	0.04	2782
2	0.30	3.81	0.25	0.02	2701	1660	"	"	"	"
3	0.40	3.31	0.22	0.02	2738	1639	"	"	"	"
4	0.54	2.59	0.18	0.03	2789	1606	"	"	"	"
5	0.49	3.84	0.26	0.02	2775	1667	0.66	0.66	0.03	2754
6	0.57	4.21	0.29	0.02	2807	1688	0.57	0.57	0.03	2737
7	0.38	4.45	0.28	0.02	2741	1680	0.79	0.79	0.04	2823
8	0.35	7.79	0.46	0.02	2744	1797	0.77	0.77	0.04	2882
9	0.40	2.45	0.18	0.02	2738	1608	0.77	0.77	0.04	2751
10	0.40	1.96	0.15	0.02	2738	1589	0.74	0.74	0.04	2729
11	0.57	3.08	0.23	0.02	2807	1648	0.55	0.55	0.03	2712
12	0.59	0.47	0.47	0.03	2806	1491	0.80	0.80	0.04	2782
13	0.40	0.66	0.66	0.02	2738	1504	"	"	"	"
14	0.56	1.87	0.78	0.02	2805	1577	0.57	0.57	0.03	2737

10. REFERENCES.

[1] Reactor Safety Study - An Assessment of Accident Risks in US Commercial Reactor Plants. WASH-1400 (also NUREG-75/014), (1975).

[2] The German Risk Study. Published by the Federal Minister of Research and Technology, (1979).

[3] Zion Probabilistic Safety Study. Commonwealth Edison Co. Docket No. 50-295, (1981).

[4] Sizewell B Probabilistic Safety Study. Westinghouse Electric Corporation, WCAP-9991, (1982).

[5] B.D. Turland and J. Morgan. Thermal Attack of Core Debris on a PWR Reactor Vessel. Proceedings of International Meeting on LWR Severe Accident Evaluation, Cambridge, (1983).

[6] B.D. Turland and J. Morgan. Progression of a PWR Severe Accident from Core Melt to Cavity Interactions. Proceedings of Fifth Information Exchange Meeting on Debris Coolability, UCLA, (1984).

[7] R.O. Wooton and H.I. Avci. MARCH (Meltdown Accident Response Characteristics) Code Description and User's Manual. NUREG/CR-1711, (1980).

[8] R.O.Wooton, P.Cybulskis and S.F.Quayle. MARCH2 (Meltdown Accident Response Characteristics Code. Description and User's Manual. NUREG/CR-3988, (1984).

[9] W.B. Murfin. A Preliminary Model for Core-Concrete Interactions. Sandia Laboratories report, SAND77-0370, (1977).

[10] J.F. Muir, R.K. Cole Jr., M.L. Corradini and M.A. Ellis. CORCON-MOD1: An Improved Model for Molten Core/Concrete Interactions. Sandia Laboratories report, SAND 80-2415 (also NUREG/CR-2142), (1981).

[11] J.H. Gittus et al. PWR Degraded Core Analysis - A Report by a Committee Chaired by Dr. J.H. Gittus. UKAEA Northern Division Report ND-R-610(s), (1982).

[12] C.Politis. Untersuchungen in Dreistoffsystem Uran-Zirkon-Sauerstoff, KfK 2167 (1975).

[13] P.Hofmann and C.Politis. The Kinetics of the Uranium Dioxide - Zircaloy Reactions at High Temperatures. Journal of Nuclear Materials, Vol.87, pp.375-397 (1979).

[14] B.D.Johnston. The Zircaloy-Uranium Dioxide Reaction. UKAEA report SRD-R-294 (1984).

[15] J. Morgan, P. Winter, B.D. Turland et al. Compendium of Post Accident Heat Removal Models for Liquid Metal Cooled Fast Breeder Reactors (Eds. B.D. Turland and J. Morgan). Report to be published by DG XII, Brussels, (1985).

[16] H.H. Reineke, R. Schramm and V. Steinberner. Heat Transfer from a Stratified Two Fluid System with Internal Heat Sources. Proceedings of Fourth Post Accident Heat Removal Information Exchange, pp1401-1411, (1979).

[17] W.H. Ruehle. On Thermal Convection in Two Immiscible Fluid Layers. Doctoral Dissertation, UCLA, (1963).

[18] F.A. Kulacki, J.H. Min, A-T. Nguyen and M. Keyhani. Steady and Transient Natural Convection in a Horizontal Layer of Two Immiscible Fluids with Internal Heat Generation. Proceedings Fourth Post Accident Heat Removal Information Exchange, pp1412-1427, (1979).

[19] F.A. Kulacki and A-T. Nguyen. Hydrodynamic Instability and Thermal Convection in a Horizontal Layer of Two Immiscible Fluids with Internal Heat Generation. NUREG/CR-2619R3, (1980)

[20] F.A.Kulacki, A.A.Emara, J.H.Min and A-T.Nguyen. Experimental Studies of Steady and Transient Natural Convection with Internal Heat Sources in Enclosed Cavities. Proc. 4th Water Reactor Research Meeting Gaithersburg (1976).

[21] R.S.Peckover. The Effect of Convection on Heat Transfer with Internal Heat Sources (part 2). UKAEA report CLM-M91 (1972).

[22] L.Baker Jr., R.E.Faw and K.A.Kulacki. Post Accident Heat Removal I: Heat Transfer Within an Internally Heated Nonboiling Liquid layer. Nuc. Sci. and Eng. Vol.61, p.222 (1976).

[23] D.L.Hagrman. Materials Properties Models for Severe Core Damage Analysis. EG&G report EGG-CDD-5801 (1982).

[24] American Nuclear Standard for Decay Power in Light Water Reactors. ANSI/ANS-5.1-1971, (1971).

[25] B.Gebhart. Heat Transfer. Published by McGraw-Hill, (1961).

[26] F.A.Kulacki and A.A.Emara. High Rayleigh Number Natural Convection in Enclosed Fluid Layers with Internal Heat Sources. NUREG-75/065, (1975).

APPENDIX A : DESCRIPTION OF INPUT DATA FOR THE TWOLAY PROGRAM.

This appendix details TWOLAY NAMELIST input and the data used in the parameter and comparison study described in section 6. All input data to the code is in SI (mks) units. The following notation is used below;

Denotes values, varied in the parameter study, described in section 5 of this paper.

** For MODEL=0 the overlying coolant model is used, whilst for all other values the radiation model is used.

Description	Variable Name	Value Used
NAMELIST NLGEN		
Fractional error in numerical calculations,	ERROR	0.0001
Time since start of accident,	TIMSTR	7200 s
Time reactor has been at power,	TIMEAP	3.1536×10^{7} s
Reactor thermal power,	QTIMEO	3400 MWt
Pseudo timestep,	DT	20 s
Radius of curvature of the hemisphere,	RPCURV	2.2 m
NAMELIST NLOX		
Fraction of total f.p. heating in oxide,	FFPOX	##
Specific heat capacity of the oxide,	CPOX	##
Mass of oxide debris	WOX	##
Oxide 'sidewards' boundary temperature,	TOXS	2550°C
Oxide 'downwards' boundary temperature,	TOXD	2550°C
Coefficient of expansion for the oxide,	BETAOX	7.4×10^{-5} per°C
Density of the oxide,	RHOOX	##
Thermal conductivity of the oxide,	CONDOX	##
Viscosity of the oxide,	VISCOX	4×10^{-3} kg/m/s
'Sidewards' oxide h.t. correlation const.,	COXS	0.345
'Sidewards' oxide h.t. correlation exponent,	GAMOXS	0.226

'Upwards' oxide h.t. correlation const.,	COXU	0.345
'Upwards' oxide h.t. correlation exponent	GAMOXU	0.226
Oxide debris melting point,	TOXMP	2550°C
Trial oxide debris temperature,	TOXIDE	2700°C

NAMELIST NLMET

Fraction of total f.p. heating in the metal,	FFPMET	##
Thermal conductivity of the metal,	CONDME	##
'Sidewards' metal h.t. correlation const.,	CMETS	0.345
Coefficient of expansion of the metal,	BETAME	1.76×10^{-5} per°C
Viscosity of the metal,	VISCME	1.58×10^{-3} kg/m/s
'Sidewards' metal h.t. correlation exponent,	GAMMES	0.226
'Upwards' metal h.t. correlation const.,	CMETU	0.345
'Upwards' metal h.t. correlation exponent,	GAMMEU	0.226
Metallic debris melting point,	TMETMP	1450°C
Trial metallic debris temperature,	TMETAL	2500°C
Specific heat capacity of the metal,	CPMET	##
Mass of metallic debris,	WMET	##
Density of metallic debris,	RHOMET	##
Metal 'sideways' boundary temperature,	TMETS	1450°C

NAMELIST NLSURF

Upper boundary condition model selection,	MODEL	**
Radiation model sink temperature,	TSINK	1450°C
Form factor in radiation model,	FORMFC	1.0
Emmissivity used in overlying coolant model,	EMISSY	1.0
Coolant saturation temperature,	TSAT	100°C
Coolant vapour viscosity,	VISCVP	4.75×10^{-5} kg/m/s
Coolant surface tension,	SURFTN	0.05878 J/m2
Density of the coolant,	RHOLIQ	960 kg/m3
Density of the vapour,	RHOVAP	0.1703 kg/m3
Latent heat of vaporisation of the coolant,	HLATVP	2.26×10^{6} J/g
Thermal conductivity of the vapour,	CONDVP	0.135 W/m/K

Available from
HER MAJESTY'S STATIONERY OFFICE
49 High Holborn, London, WC1V 6HB
(Personal callers only)
P.O. Box 276, London, SE1 9NH
(Trade orders by post)
13a Castle Street, Edinburgh, EH2 3AR
41 The Hayes, Cardiff, CF1 1JW
Princess Street, Manchester, M60 8AS
Southey House, Wine Street, Bristol, BS1 2BQ
258 Broad Street, Birmingham, B1 2HE
80 Chichester Street, Belfast, BT1 4JY

PRINTED IN ENGLAND

CLM-R262

CLM-R262

UKAEA

Report

CURLIM

A RATE LIMITED MCFI MODEL FOR SODIUM

Part I: Fundamental Model and Parameter Studies

D. F. FLETCHER

CULHAM LABORATORY
Abingdon Oxfordshire
1986

C.18

Available from H. M. Stationery Office

Price £5.00